Fluxon lattice oscillations in layered superconductors

S. E. Shafranjuk*
Research Institute of Electrical Communication, 2-1-1 Katahira, Aoba-ku, Sendai 980-77, Japan

M. Tachiki
National Research Institute for Metals, 1-2-1 Sengen, Tsukuba 305, Japan

T. Yamashita
Research Institute of Electrical Communication, 2-1-1 Katahira, Aoba-ku, Sendai 980-77, Japan
(Received 6 June 1997; revised manuscript received 14 November 1997)

The fluxon structure in a layered superconductor under an applied parallel constant magnetic field is examined within the model of stacked Josephson junctions. The interlayer phase difference $\varphi_{n,n+1}$, which is found as a solution of the system of nonlinear equations, corresponds to buckled chains of fluxons, alternating with the field strength. The calculated $\varphi_{n,n+1}$ is then used to obtain the spectrum of vortex and plasma small oscillations that has a fine band structure showing gaps.
[S0163-1829(98)03722-9]

I. INTRODUCTION

The attention paid to the intrinsic Josephson effect (IJE) in the metal oxide superconductors is prompted by numerous interesting experimental data obtained in recent years. After the discovery of the IJE itself,[1] the next spectacular example was the observation of a low-lying collective mode in c polarized experiments[2–4] made on single crystal samples. A theoretical interpretation[5–7] of the mentioned results is based on the idea of a weak Josephson coupling between superconducting CuO_2 layers separated by nonconducting interstitial regions $\mathcal{I}$. This means that metal oxide single crystal samples behave like a stack of microscopic tunneling junctions[1] $\cdots CuO_2$-$\mathcal{I}$-$CuO_2\cdots$. This kind of setup particularly determines the electrodynamic properties[5] of these materials in a mixed state created by an applied constant magnetic field.[6,7] Under certain conditions (which basically depend on many factors, e.g., temperature, field strength, and anisotropy parameter) the mixed state may consist of a regular set of vortex lines. Depending on the orientation of the external field $\mathbf{B}$ various vortex structures that may appear in a layered superconductor (SC) can be reduced to two important limiting cases.[8–10] When the field is parallel to the layers, i.e., $\mathbf{B}\|ab$ planes, the structure is formed by Josephson vortices, fluxons, while in a perpendicular field it can consist of a set of pancakelike structures. Since the mixed state corresponds to a minimum of the total thermodynamic potential at $\mathbf{B}\neq\mathbf{0}$, one may consider small oscillations near the equilibrium position, which are analogous to plasma and vortex oscillations of a fluxon lattice in a single long Josephson junction.[11] However, in metal oxide SC's, due to the interlayer coupling, the $\cdots CuO_2$-$\mathcal{I}$-$CuO_2\cdots$ junctions can be supposed to be no longer independent; thus the single-junction solution[11] may not be adequate for the stack. This means that in layered SC's, the steady state fluxon lattice[11] may have specific features that make it different from both an isotropic homogeneous SC's and a single junction. Since until now only the limiting cases of either a strong or a weak magnetic field were considered, there arises a fundamental question as to which kind of mixed state occurs in an arbitrary parallel field for a big stack of Josephson junctions. Another point that is addressed is a dispersion law for the modes of a fluxon lattice, which may have a complex multiband anisotropic structure. Because the Josephson properties themselves are quite dependent on the strength of magnetic field, another issue here concerns the relationship between the Josephson oscillations[5] and the presence of the vortex structure. Calculations of the resonance frequency were performed for cases of parallel and tilted fields in recent papers.[6,7] Nevertheless, the results[6,7] were obtained only for limits of weak or strong fields, while an important case of arbitrary field amplitude remained to be solved. An additional restriction[6,7] concerned the structure of the mixed state, which was assumed to be a triangular (or hexagonal) fluxon lattice. The triangular fluxon arrangement was claimed to take place also in stacks of a few ($N=5$) junctions in Refs. 12. However, the size of the stack there[12] was too small to relate it to a bulk crystal. Additionally, Pedersen and co-workers[12–14] neglected the interplane recharging effect (see, e.g., Refs. 7 and 15), which is of crucial importance for nonstationary phenomena.

In this paper we examine which kind of fluxon structure takes place under an arbitrary magnetic field applied parallel [$\mathbf{B}\|ab$ planes] to a stack of Josephson junctions. The steady fluxon state obtained here is used to explore the spectrum of plasma and vortex small oscillations. In Sec. II we discuss the main assumptions of the model and formulate basic equations. In order to find the interlayer phase difference describing a fluxon lattice, we obtain a numerical solution for a system of nonlinear equations. We show that the kind of solution depends on the field strength and parameter of anisotropy between the c axis and ab planes. In Sec. III, beginning with a simple model of a layered SC for an interesting limiting case, we consider the excitation spectra Ω_k of small oscillations. Using results obtained for the fluxon lattice in Sec. II, we also perform numerical calculations of

Ω_k. We obtain that the spectrum of plasma excitations has a band structure determined by the strength of the magnetic field **B** as well as by the interlayer coupling and the anisotropy of the penetration depth. The branches Ω_k have regions with negative group velocity $v_k<0$ and are separated by gaps. The interaction between the junctions leads to c axis fluxon oscillations with a peculiar dispersion law. The ab plane branches also have a different and more complex structure in comparison to the case of the one-dimensional long Josephson junction.[11]

II. FLUXON LATTICE IN THE SET OF STACKED JUNCTIONS

The gestalt of the vortex state, taking place in metal oxide superconductors, basically depends on several factors such as the magnitude of the external magnetic field **B**, the strength of the interlayer coupling, the anisotropy parameter γ, and the temperature T. The theoretical models for the vortex state in a weakly coupled layered SC were initially proposed in Refs. 6 and 8–10. As it was emphasized in Refs. 8–10, the alternation of the order parameter amplitude $|\Delta(\mathbf{r})|$ does not contribute essentially to the total free energy, particularly in a parallel field ($\mathbf{B}\|ab$ planes), because the vortex cores are localized in interlayer regions. The equations for the order parameter in a layered SC with the Josephson coupling follow from the free energy functional[8–10] describing the SC in a magnetic field or from Maxwell equations taking into account the Josephson relationship. This kind of equation was used before (see, for instance, Refs. 6 and 8–10) to determine the interlayer phase difference $\phi_{n,n+1}$. However, even for a well-defined fluxon lattice, which we explore here, the solutions $\phi_{n,n+1}$ had been obtained, until now, only in limiting cases, although a moderate field strength is a matter of interest. In the stacked system, the equation for interlayer phase differences $\phi_{n,n+1}$ reads (see, e.g., Refs. 7)

$$\nabla_{\|}^2\phi_{n,n+1}-\frac{1}{\lambda_J^2}(2\sin\phi_{n,n+1}-\sin\phi_{n+1,n+2}-\sin\phi_{n-1,n}) - \frac{1}{\lambda_\perp^2}\sin\phi_{n,n+1} = \frac{\epsilon}{c^2}\frac{\partial^2}{\partial t^2}\left[\phi_{n,n+1}+\frac{\lambda_\perp^2}{\lambda_J^2}(2\phi_{n,n+1}-\phi_{n+1,n+2}-\phi_{n-1,n})\right], \tag{1}$$

where $n=\overline{0,\ldots,N}$ denotes the layer's index, N is the number of layers in the stack, $\lambda_J=\gamma c_\perp$, $c_\perp$ is the c axis lattice constant, $\gamma=\lambda_\perp/\lambda_\|$ is the anisotropy ratio, $\lambda_\perp$ and $\lambda_\|$ are the static penetration depths along the c axis and the ab plane, respectively, $\nabla_\|^2$ is the Laplacian along ab planes, and $\nabla_\|^2=\nabla_x^2+\nabla_y^2$. In metal oxides, the anisotropy ratio is typically large $\gamma=100-1000$ (see, e.g., Ref. 1). This means that the second term on the left-hand side of Eq. (1), which is due to a mutual influence between neighbor junctions in the stack, may prevail over the third term (which is caused by the Josephson current within the same junction). A similar equation had been derived in Refs. 12 and 14, but they omitted the term in parentheses on the right-hand side of Eq. (1), which essentially contributes to a nonstationary case due to the big coefficient $(\lambda_\perp/\lambda_J)^2=10^4-10^6$. Let us also note that Bulaevskii *et al.* used a more compact form of Eq. (1), but, in fact, they sacrificed a generality, initially assuming the dispersion relationship such as $k=\omega/\overline{c}$. Another problem is related to the dynamic screening effects, which were included in an equation of Ref. 7 in a static case. Therefore, we prefer to begin with Eq. (1) rather than with the equation of Ref. 7.

With respect to Eq. (1), indeed, there exists a complication that appears due to finite differences. It serves as a reason why this equation has such a distinct mathematical background compared, e.g., to the case of a long Josephson junction.[11] The right-hand side of Eq. (1) contributes only to a nonstationary case and is modified here to be consistent with the conservation condition $\partial\rho/\partial t+\nabla\mathbf{j}=0$ (ρ and $\mathbf{j}$ are the electric charge and current density, respectively). Small oscillations of the fluxon lattice can be expressed as an ac addition $\varphi_{n,n+1}^{(1)}(t)$ to the ''vortex'' phase difference $\varphi_{n,n+1}$,

$$\phi_{n,n+1}(t)=\varphi_{n,n+1}+\varphi_{n,n+1}^{(1)}(t), \tag{2}$$

where $\varphi_{n,n+1}^{(1)}(t)$ may also be attributed to an ac field by the Josephson relationship

$$\varphi_{n,n+1}^{(1)}(t)=\frac{2ed}{\hbar}\int^t dt\, E_z(t), \tag{3}$$

where d is the averaged thickness of interstitial regions, $d\simeq c_\perp$, and $E_z(t)$ is the c axis component of the electric field vector. In the following we will be interested in a steady state vortex solution. Then Eq. (1) has to be completed by boundary conditions (BC's) that determine the positions of the vortices. Bulaevskii *et al.*[6,7] suggested that in a parallel dc magnetic field, the centers of vortices form a triangular lattice of fluxons,[10] the parameters of which are established by the requirement that the magnetic flux is Φ_0 per vortex. Assuming also that in a general case the fluxon lattice may contain the vortices not in every adjacent layer but, e.g., in every lth layer, they introduced the commensurability parameter l, which is an integer number. In a weak magnetic field (which, following Ref. 10, corresponds to $a_x>\lambda_J$, where a_x is the vortex lattice constant along the a axis) it gives the lattice period as $2lc_\perp$ in the c direction and $a_x=\Phi_0/Blc_\perp$ in the a direction. In a strong field[10] $a_x<\lambda_J$ the vortex cores fill all the interlayer regions. Asymptotic solutions for the aforementioned limiting cases were found in Ref. 6. Numerical nonstationary solutions for a stack of five Josephson junctions obtained in Refs. 12–14, however, neglect a recharging effect, which may affect the vortex dynamics drastically.

In this paper we consider the case of an arbitrary field, using a numerical solution of Eq. (1). Equation (1) was treated as a system of N second-order equations for a finite number of layers N, which is then reduced to a system of $2N$ first-order equations. To solve Eq. (1) we used BC's of the following form. Since in metal oxides the values of λ_J are 2–3 orders smaller than in long Josephson junctions formed by classic superconductors, one has to modify the BC's for the former case. In particular, for a vortex lattice, one can use BC's that reflect the periodic variation of the local field in

space and a periodic distribution of the supercurrent density inside the sample along x. Here we assume that the external magnetic induction $\mathbf{B}=(0,B_y,0)$ is homogeneous outside the stack of junctions. However, inside the stack it may become nonuniform due to the presence of vortices. In a steady state, the distribution of induction can be found from the Maxwell equation and is related to the interlayer current $j_{z,n}$ as

$$\nabla_x B_y^{(n)}(x)=\frac{4\pi}{c}j_{z,n}, \tag{4}$$

where $B_y^{(n)}(x)$ is the $\hat{y}$ component of the induction in the layer n, which depends on the a axis coordinate x. Actually, we apply BC's at the edges of each elementary cell instead of to the whole sample, i.e., fixing gradients of the phase difference at x_l (x_r) [the left (right) edge of the unit cell]. Nevertheless, to perform a numerical integration we have to follow a self-consistent solution. It is achieved in the following way. As an initial step we introduce fluxons to a set of junctions $n+l$ (n is the junction's index and l is an integer number) by applying BC's

$$(\varphi_{n+l,n+l+1})_{x=x_l}=\pi, \quad \left(\frac{\partial\varphi_{n+l,n+l+1}}{\partial x}\right)_{x=x_l}=\Xi_0, \tag{5}$$

where $\Xi_0=(2ec_\perp/\hbar)B_{uc}$, with B_{uc} the value of induction at the edges of the unit cell, which, generally speaking, has to be found from a normalization condition self-consistently (see below). We also assumed that $\delta_n^{(1)}j_{x,n}=0$, where $\delta_n^{(1)}$ means the first-order finite difference operator. In all the other layers $n+k$ ($k\neq l$) we use

$$(\varphi_{n+k,n+k+1})_{x=x_l}=0, \quad \left(\frac{\partial\varphi_{n+k,n+k+1}}{\partial x}\right)_{x=x_l}=\Xi_0, \tag{6}$$

respectively. Then we perform the integration along the x coordinate, e.g., from $x=x_l$ to $x=x_r=x_l+a_x$. At the last point we reverse the integration with descending x back to $x=x_l$, implementing BC's

$$\left(\frac{\partial\varphi_{n,n+1}}{\partial x}\right)_{x=x_r}=\Xi_0, \tag{7}$$

while for $(\varphi_{n,n+1})_{x=x_r}$ we use the value obtained from the previous ascending integration. Then we repeat the procedure with ascending and descending x coordinates until a stable solution has been achieved. Of course, BC's are different for various types of vortex structure and basically must be verified by a corresponding calculation of thermodynamic potential, which has to be minimized in order to find a stable configuration. These BC's are then used for a numerical solution of Eq. (1), which for convenience can be reduced to a system of $2N$ differential equations with respect to x. We begin with a stack of $N=15$ junctions. In this case, with BC's (5) and (6), we do not get any stable solution for $\varphi_{n,n+1}(x)$. Contrary to our initial expectations and to Ref. 12 (where static results were reported for $N=5$; see, e.g., Fig. 5 therein), we obtain a triangular lattice only for some particular field amplitude, which disarranges as the field changes. However, when the number of junctions in the stack is increased up to $N=50$ (and higher), the situation becomes different, showing a regular array of fluxons. In three-dimensional (3D) plots of Figs. 1–5 we present typical solutions $\varphi_{n,n+1}(x)$ versus the layer index n and the a axis coordinate x at the strength of the parallel field $B_y=0.03$ obtained for $N=50$; $\lambda_\perp=2$ and $\lambda_J=0.02$ for various l. We express B_y in units of $\Phi_0/\eta c_\perp^2$ (Φ_0 being the elementary magnetic flux and $\eta=5\times10^3$), while the length is expressed in units of $0.5\times10^4 c_\perp$. If one accepts, e.g., the value $c_\perp \simeq 1$ nm, then $\Phi_0/\eta c_\perp^2=0.4$ T. These unusual units were chosen because an important spatial alternation in the system takes place on the scale $\sim\lambda_\perp$, while a more fundamental scale is $\sim c_\perp$. The self-consistent procedure to determine the induction at $x=x_{l,r}$ is the following. Initially we solve Eq. (1) with BC's (5) and (6) setting $B_{uc}=B_y$. Then we calculate the interlayer supercurrent distribution proportional to $\sin[\varphi_{n,n+1}(x)]$, from which, using the Maxwell equation (4), one finds the variation of the local magnetic induction in space $B_n^{loc}(x)$. It is checked whether the function $B_n^{loc}(x)$ satisfies the condition for the total flux across the stack, which is

$$\sum_n \int_0^{L_x} dx\ B_n^{loc}(x)=B_y N L_x, \tag{8}$$

where L_x is the length of the sample and N is the number of junctions in the stack. If the left-hand side of Eq. (8) deviates from $B_y N L_x$, then for the next cycle B_{uc} should increase (or decrease) until self-consistency is achieved. The detailed calculations conducted here show that the final result, however, is not very sensitive to the precise value of B_{uc}; therefore, for practical reasons we set simply $B_y=B_{uc}$. From the figures mentioned one can notice that there is a regular fluxon structure which nevertheless depends on the value of the commensurability parameter l. In the aforementioned plots, the position $[X_i,N_i]$ of a fluxon core is determined by the conditions

$$\varphi_{n,n+1}(x)=0 \quad \text{at} \quad \delta_n^{(1)}\left[\frac{\partial\varphi_{n,n+1}}{\partial x}\right]_{x=X_i,n=N_i}\neq 0. \tag{9}$$

From Fig. 1 ($l=2$, i.e., the phase difference at x_l is of the form $\ldots.00\pi00\pi00\ldots$) one can see that instead of a triangular lattice the fluxons form a buckled V-shaped structure. The buckled chains are sensitive to the value of l. In reality, as one can see from Fig. 2, plotted for $l=3$, the fluxon structure tends to reorder. In this figure one can observe a creation of chain with an opposite orientation of buckling. This process continues as l increases; thus the fluxons become rearranged again (see, e.g., Fig. 3), forming a rhomblike structure composed of two buckled chains with opposite inclining angles. The arrangement is even improved as l increases up to $l=5$ (see Fig. 4). In this case the V-shaped structure has an orientational opposite to that taking at $l=2$. However, the array at $l=6$ (which is shown in Fig. 5) is ordered much better, but in this case a_x becomes pretty small and only a few fluxons could fit in the unit cell.

Our calculations show that when the field strength is increased at fixed l (which means that the size of the ''cell'' along the x axis, $a_x=\eta c_\perp/Bl$ in the units used here, is decreased), the evolution of the fluxon structure depends on the value of l. The tendency is that the fluxon structure becomes

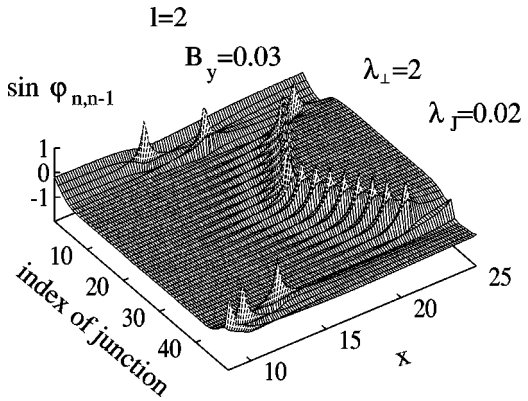

FIG. 1. Interlayer Josephson current $\sin[\phi_{n,n+1}(x)]$ calculated for a stack ($N=50$) of Josephson junctions in the parallel field $B=0.03$, $l=2$.

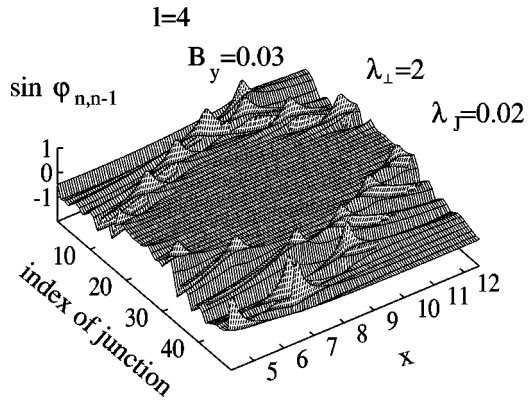

FIG. 3. Intermediate state of the vortex array at $l=4$. One can notice the rhombic shape of the structure.

more arranged as the field grows. Another remarkable feature that is evident from Figs. 1–5 is the size of an individual fluxon. From the numerical solution we find that this typical size is $\sim\lambda_\perp$, but not λ_J (compare with Ref. 6) and it is not scaled to the whole size of the sample (compare with Refs. 12 and 14). The above calculations performed for various BC's show that a stable solution may be selected with regard to minimal energy. The calculation of the averaged Josephson energy $E_J \propto \langle 1-\cos\varphi_{n,n+1}\rangle_{sample}$ for different l shows a general tendency that E_J grows as B_y and l decrease. The odd l are more energetically profitable in comparison to even l. However, the Josephson energy itself, due to the huge anisotropy, is much smaller in comparison to the interfluxon energy within the ab plane. On the contrary, the interplane distance $c_\perp$ is much smaller in comparison to the typical length of fluxons ($\sim\lambda_\perp$) along the x axis, which overlap if the field is sufficiently strong (then $a_x\sim\lambda_\perp$). The interfluxon interaction indeed is repulsive. It is confirmed by the introduction of only two fluxons in our sample. Independently from the point of entry, they are pushed out to the opposite edges ($n=1$ and $n=50$) of the stack. The aforementioned serve as reasons for a dramatic competition between different factors, responsible for the formation of the fluxon chain. One can see that the expected triangular lattice does not occur for the BC's used. It is not achieved even if one tries to push more fluxons into the stack, e.g., by applying boundary conditions such as $\ldots\pi\pi0\pi\pi0\pi\pi\ldots$. Although the commensurability parameter ''l'' traditionally was stated as an integer in several previous papers (see, e.g. Refs. 6–10), we formally may introduce a noninteger magnitude $l=1/2$ to describe the boundary condition $\ldots\pi\pi0\pi\pi0\pi\pi0\pi\pi0\ldots$. Decreasing l, one may achieve a structure with more than one fluxon per layer, but even this sort of effort does not lead to a triangular lattice.

Additional calculations show that the data for the stacks with 50 and 100 junctions are similar. They both give the buckled chain solution with a little distinction in the positions of a few fluxons at the edges ($n=0$ and $n=50$ for a 50-junction stack and $n=0$ and $n=100$ for a 100-junction stack). For instance, in Fig. 1 the mentioned fluxons that drop out of the chain are located at $n=2$ and 5 (the edge $n=0$) and at $n=46$, 48, and 50 (the edge $n=50$). Similarly, at $l=5$ there is also a fluxon (in Fig. 4 it is positioned at $n=5$ and $x=9.5$), which drops out from the common array. The calculations conducted for the 100-junction stack also give the buckled chain of fluxons, although a few fluxons drop out of the chain near the edges $n=0$ and $n=100$ as well. The alternation of cell size along the x direction a_x by varying the magnetic induction B_y at other fixed parameters results mostly in the rescaling of the $\varphi_{n,n+1}(x)$ surface while qualitative changes of the shape of it are small.

The above calculations suggest that the position and the inclining angle of a chain depend mainly on the number of fluxons introduced in the stack initially (which in our terms

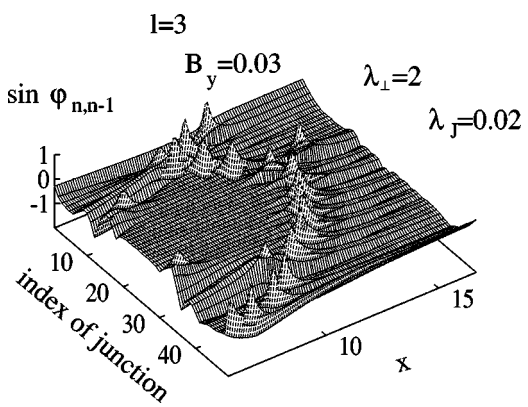

FIG. 2. Same dependence as in Fig. 1, but $l=3$. One can observe that the fluxon structure begins to reorder.

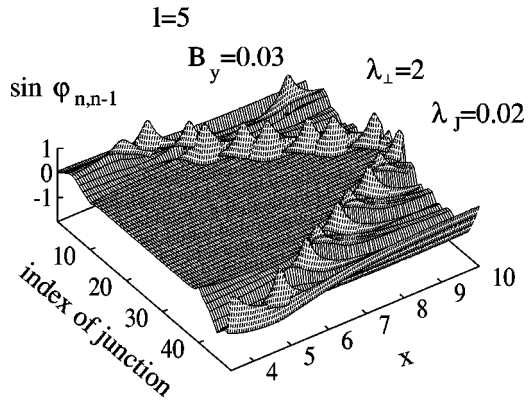

FIG. 4. At $l=5$ the structure is already arranged in the opposite way, except for one fluxon that drops out (it belongs to a chain in another unit cell).

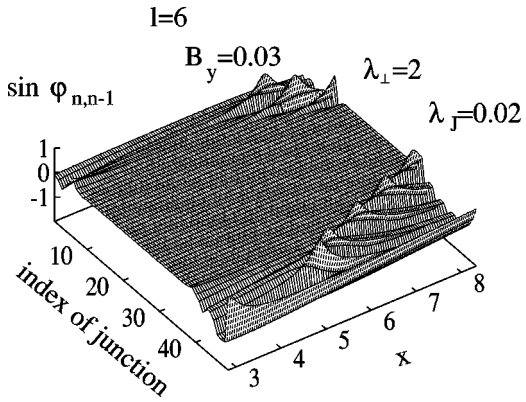

FIG. 5. When $l=6$, the size of the cell becomes pretty small and only a few fluxons can fit in the cell.

is related to the parameter l) and are not very sensitive to the shape of the initial input. However, a stable profile $\varphi_{n,n+1}(x)$ is obtained after several cycles (in most cases three to four cycles give already a good profile) of the reversal integration. Varying BC's, we checked the symmetry and size dependences of the fluxon chains. We found that there is no basic symmetry in the n direction, although BC's along n are periodic inside the stack. However, the solutions obtained are always similar, although depending on BC's, the buckled chains are shifted or may have a negative inclining angle (compare Figs. 1 and 4). In some cases one obtains a combination of two chains with opposite inclining angles (see Figs. 2 and 3). Similar buckled chains of vortices were observed by means of the Bitter-pattern technique in Ref. 16 for a $Y_1Ba_2Cu_3O_7$ single crystal sample in a parallel magnetic field. Although the initial interpretation[17] of the experiment[16] was given in terms of Abrikosov vortices, considering it within the phenomenological London model, in our opinion, this kind of approach[17] is highly controversial for the layered superconductor with an intrinsic Josephson effect. Instead, the application of the Lawrence-Doniach model is more logistic in this case. These results are connected with the strong anisotropy and nonlinear properties of the system that is essentially distinct from the case of Abrikosov vortices.

III. SMALL OSCILLATIONS OF THE FLUXON LATTICE

In this section we consider the spectrum of small oscillations of the fluxon lattice using stationary solutions of Eq. (1). The time evolution of fluxons can be described by quantizing the classical field equations in a way similar to that for a single junction in Ref. 11. The total Hamiltonian operator for the stacked set of Josephson junctions, like the single-junction Hamiltonian,[11] basically contains harmonic and anharmonic terms. When deviations from equilibrium are small, the anharmonic terms are negligible[11] and the nonstationary effect is reduced to small fluctuations. Therefore, one can consider elementary excitations in this system, with a steady ground state characterized by $\varphi_{n,n+1}$. This kind of oscillation at $\varphi_{n,n+1}\equiv 0$ is similar to that[5] obtained for the case $\mathbf{B}\equiv\mathbf{0}$. Due to the essential interlayer interaction, the system becomes three-dimensional, which is different from the setup of Ref. 11. Therefore, the case of a long Josephson junction[11] (where $\lambda_\perp$ is finite while $\lambda_J\to\infty$) is somehow opposite to our situation, which rather corresponds to $\lambda_\perp \gg \lambda_J$. Here, using the equation for the stacked system of Josephson junctions (see, e.g., Ref. 7), we investigate the 3D setup. Equation (1) can be linearized with respect to small deviations $\varphi^{(1)}_{n,n+1}$ as

$$\nabla_\parallel^2\varphi^{(1)}_{n,n+1}-\overline{c}^{-2}\frac{\partial^2}{\partial t^2}\times\left[\varphi^{(1)}_{n,n+1}+\frac{\lambda_\perp^2}{\lambda_J^2}(2\varphi^{(1)}_{n,n+1}-\varphi^{(1)}_{n+1,n+2}-\varphi^{(1)}_{n-1,n})\right]=j^J_{Jos}(t)+j^\perp_{Jos}(t)+j^{qp}(t), \tag{10}$$

where $\overline{c}=c/\sqrt{\epsilon}$ (ϵ is the dielectric constant of the barrier and c is the velocity of light in vacuum). The right-hand side of Eq. (10) consists of driving terms, where

$$j^J_{Jos}=\frac{1}{\lambda_J^2}[2\varphi^{(1)}_{n,n+1}\cos\varphi^{(0)}_{n,n+1}-\varphi^{(1)}_{n+1,n+2}\cos\varphi^{(0)}_{n+1,n+2}-\varphi^{(1)}_{n-1,n}\cos\varphi^{(0)}_{n-1,n}] \tag{11}$$

is the linear part of the ac Josephson contribution along the c axis, while

$$j^\perp_{Jos}=\frac{1}{\lambda_\perp^2}\varphi^{(1)}_{n,n+1}\cos\varphi^{(0)}_{n,n+1} \tag{12}$$

is the corresponding in-plane ac part. The third term on the right-hand side of Eq. (10) belongs to a contribution from the quasiparticles that exist, e.g., for an anisotropic pairing case[5] even at low temperatures and at low frequencies. Using the substitution

$$\varphi^{(1)}_{n,n+1}=\exp\{ik_y y+ik_z nc_\perp-i\omega t\}f_n(x) \tag{13}$$

and the ''potential'' $\cos\varphi^{(0)}_{n,n+1}=U_n(x)$, Eq. (10) can be reduced to the system of Schrödinger-like equations

$$(\nabla_x^2-k_y^2)f_n(x)=\frac{1}{\lambda_J^2}\left\{2\left[U_n(x)-\frac{\omega^2}{\overline{c}^2}\lambda_\perp^2\right]f_n(x)-e^{ik_zc_\perp}\times\left[e^{-iGa/2}U_{n-1}(x)-\frac{\omega^2}{\overline{c}^2}\lambda_\perp^2\right]f_{n-1}(x)-e^{-ik_zc_\perp}\times\left[e^{iGa/2}U_{n+1}(x)-\frac{\omega^2}{\overline{c}^2}\lambda_\perp^2\right]f_{n+1}(x)\right\}+\frac{1}{\lambda_\perp^2}\left[U_n(x)-\frac{\omega^2}{\overline{c}^2}\lambda_\perp^2\right]f_n(x). \tag{14}$$

Unfortunately, in the case $\lambda_\perp\gg\lambda_J$, as in Ref. 11, a general solution is not available anymore and one has to consider a numerical solution. Because numerical procedures are not always well illustrative, we would like to begin with a simple limiting case that could be solved analytically and is useful for understanding the common scenario. If one approximates the potential $\cos\varphi^{(0)}_{n,n+1}$ by a single harmonic $\sim\cos Qx$, where Q serves as a fitting parameter, the alternation of interlayer

phase difference along the a axis may be presented in the form $\varphi^{(0)}_{n,n+1}=\alpha_n x+\beta_n$. Then one can implement a two wave approximation (see, e.g., Ref. 18) with the trial function

$$f_n(x)=e^{ik_x x}a_{k_x}+e^{i(k_x-G)x}a_{k_x-G}. \tag{15}$$

Then, using periodicity conditions along the c axis and formula (15), from Eq. (14) one obtains the secular equation $\det\hat{M}=0$, where det is a determinant of the matrix $\hat{M}$ by size 6×6,

$$\hat{M}=\begin{pmatrix} \varpi_k^2 & -U_a & \varsigma\omega^2 & U_b & \varsigma^*\omega^2 & U_c \\ -U_a & \varpi_{k-G}^2 & U_b & \varsigma\omega^2 & U_c & \varsigma^*\omega^2 \\ \varsigma^*\omega^2 & U_c & \varpi_k^2 & -U_a & \varsigma\omega^2 & U_b \\ U_c & \varsigma^*\omega^2 & -U_a & \varpi_{k-G}^2 & U_b & \varsigma\omega^2 \\ \varsigma\omega^2 & U_b & \varsigma^*\omega^2 & U_c & \varpi_k^2 & -U_a \\ U_b & \varsigma\omega^2 & U_c & \varsigma^*\omega^2 & -U_a & \varpi_{k-G}^2 \end{pmatrix}, \tag{16}$$

where $\varpi_k^2=(\bar{c}k_\parallel)^2-\omega^2[1+\beta^{-2}]$; $\varpi_{k-G}^2=(\bar{c}k_{\parallel-G})^2-\omega^2[1+\beta^{-2}]$, $k_\parallel=\sqrt{k_x^2+k_y^2}$; $k_{\parallel-G}=\sqrt{(k_x-G)^2+k_y^2}$; $\varsigma=\beta^{-2}e^{ik_z c_\perp}$; $\beta=\lambda_J/\sqrt{2}\lambda_\perp$, and

$$U_a=2\Omega_{cl}^2[1+\beta^2],\quad U_b=\Omega_{cl}^2 e^{ik_z c_\perp - iGa/2},\quad U_c=(U_b)^*, \tag{17}$$

where $\Omega_{cl}=\bar{c}/\lambda_J$ coincides with the classic Josephson plasma frequency; the potentials U_a, U_b, and U_c in fact determine the range for the plasma excitation spectrum. One finds the following analytical expressions for the excitation frequencies:

$$\begin{aligned}\Omega_k^{(1,2)}=\frac{1}{2}[&2\,\zeta_2+4\,\rho_1+4\,\rho_2+2\,\zeta_1 \\ &\pm 2(\zeta_2{}^2-2\,\zeta_2\zeta_1+\zeta_1{}^2+8\,U_bU_c+4\,U_b^2 \\ &-8\,U_aU_c-8\,U_aU_b+4\,U_c^2+4\,U_a^2)^{1/2}]^{1/2},\end{aligned} \tag{18}$$

where $\zeta_1=(\bar{c}k_\parallel)^2-(\bar{c}k)^2[1+\beta^{-2}]$, $\zeta_2=(\bar{c}k_{\parallel-G})^2-(\bar{c}k)^2[1+\beta^{-2}]$, $k=\sqrt{k_\parallel^2+k_z^2}$, $\rho_1=(\bar{c}k/\beta)^2e^{ik_z c_\perp}$, and $\rho_2=\rho_1^*$. From formula (18) one can see that the excitation frequency is determined by several terms $\sim(\bar{c}/\lambda_J)(k\lambda_\perp)$ (if one considers wave vectors $k\sim\lambda_\perp^{-1}$, it roughly coincides with the classic Josephson plasma frequency). Unfortunately, other eigenvalues as well as eigenvectors cannot be expressed analytically and must be obtained numerically.

However, the above approach serves as a useful introduction to the numerical procedure that we shall apply to consider a more general form of the potential $U_n(x)$. In particular it assumes that the above excitation spectra must be found for a ground state $\varphi_{n,n+1}(x)$. The last function $\varphi_{n,n+1}(x)$ was calculated from Eq. (1) for the vortex part of the interlayer phase differences, in Sec. II. Now implementing $\varphi_{n,n+1}(x)$, we conduct more general calculations of the small oscillations spectrum. Thus we go beyond the previously made harmonic approximation for the potential $\mathcal{U}_n(x)$. As in Sec. II, here we use Eqs. (10)–(12), but with the generalized potential $\mathcal{U}_n(x)=\cos[\varphi_{n,n+1}(x)]$. In this way, we calculate the coefficients $\mathcal{U}_n^s$ of the Fourier series

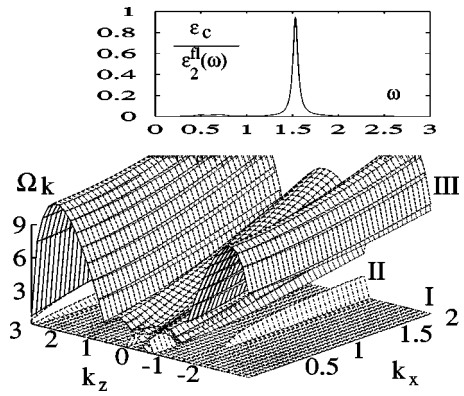

FIG. 6. Results of numerical calculations for the small oscillations. One can clearly see three bands separated by gaps. The inset at the top shows the absorption for the fluxon structure shown in Fig. 1.

$$\mathcal{U}_n(x)=\sum_s \mathcal{U}_n^s e^{i(\pi s/\alpha)x} \tag{19}$$

for any particular solution $\varphi_{n,n+1}(x)$ at given parameters N, B, $\lambda_\perp$, and λ_J. Then we approximate the solution by a linear combination of a finite number of plane waves similar to Eq. (13), but instead of Eq. (15) with

$$f_n(x)=\sum_s^L e^{i(k_x-G^s)x}a_{k_x-G^s}, \tag{20}$$

where $G^s=\pi s/a$, s is an integer number, and L is the number of waves. The substitution of Eqs. (13), (19), and (20) into Eqs. (10), (11), and (12) results in a secular equation such as $\det\hat{M}=0$. However, the size of the matrix $\hat{M}$ in this case may be much larger than 6×6 [cf. Eq. (16)]; thus the obtainment of its eigenvalues and eigenvectors requires a numerical procedure. As a result of corresponding calculations for $L=8$ one gets the branches of excitation energy $\Omega_k^{(i)}$, which are shown in the 3D plot of Fig. 6. Indeed, Fig. 6 corresponds to a superposition of fluxons from all the layers (i.e., to the structure shown in Fig. 1, where $B=0.03$, $l=2$, $\lambda_\perp=2$, and $\lambda_J=0.02$). In addition, because the plotting of all the branches in the same figure is technically problematic, in Fig. 6 we present only several branches, sufficient for illustration. The wave vector k_z is expressed in units of $c_\perp^{-1}$ and is in the range $-\pi<k_z<\pi$, the wave vector k_x is expressed in units of a_x^{-1}, and the excitation frequency is expressed in units of $\Omega_0=\bar{c}/\lambda_\perp$. All the surfaces $\Omega_k^{(i)}$ are grouped in bands, while the bands are separated by gaps. The lower band I does not have a gap and the excitation frequency is almost zero. Band II has maxima at some values of the wave vector $\mathbf{k}$, while band III strongly depends on $\mathbf{k}$ and varies within a wide range between Ω_0 and $\sim\Omega_0/\beta$. The strong dispersion of Ω_k at finite $\mathbf{k}$ particularly may contribute to losses of scaling of $B\cos\theta$ near the parallel field.[19] Indeed, the situation shown is somewhat idealized and is related rather to a well ordered structure (see, e.g., Figs. 1 or 5) assuming that the dc field is parallel only. However, any

kind of disorder (e.g., as in Fig. 2) washes out the separation between the bands or at least substantially broadens (as in Fig. 3) it. The presented dispersion law in the stacked system differs from that taking place for a fluxon lattice in a single long Josephson junction.[11] We note that, in accordance with Figs. 1–5, the interlayer phase difference $\varphi_{k,k+1}(x)$ is modified as the dc magnetic field alternates. This means that the spectrum of small oscillations changes as well.

The presence of several branches $\Omega_k^{(i)}$ in the excitation spectrum raises a question about how they contribute to observable characteristics. Therefore, we calculate here the dynamic dielectric function $\epsilon(\omega)$. The oscillating fluxons are attributed to the ac electric field by the Josephson relationship (3), which can be rewritten as

$$E_z(t)=\frac{\hbar}{2ec_\perp}\frac{\partial\varphi_{n,n+1}^{(1)}(t)}{\partial t}. \tag{21}$$

This field interacts with an external ac electric induction $D_z(t)$. Using Maxwell's equations, the ratio $\langle E_z(t)/D_z(t)\rangle_{spl}$ [which itself is related to the dielectric function $\epsilon(t)$; $\langle\ \rangle_{spl}$ is the average over the sample] can be expressed via eigenvalues and eigenvectors of the matrix $\hat{M}$. Acting in this way, we find an expression for the absorption as

$$\mathrm{Im}\left[\frac{\epsilon_\infty}{\epsilon(\omega)}\right]=\left\langle\frac{E_z(x,\omega)}{D_z(\omega)}\right\rangle_{spl}=\Gamma\omega^2\sum_{j=1}^{Q}\frac{f_j^2}{(\omega^2-[\Omega_0^{(j)}]^2)^2+\Gamma^2}, \tag{22}$$

where ϵ_∞ is the high frequency dielectric constant, Q is the number of eigenvalues (or the rank of the matrix), $f_j=\sum_{i=1}^{Q}a_0^{ij}$, a_0^{ij} is the component of the eigenvector related to the eigenvalue $\Omega_0^{(j)}=\Omega_{k=0}^{(j)}$ [there are Q components for each $\Omega_0^{(j)}$; in formula (22) the wave vector $\mathbf{k}=0$], and Γ is the resonance width that is determined by lattice disorder and/or by coupling to quasiparticles at finite temperatures. The calculation of the absorption function (22) performed here shows no contribution of the branches $\Omega_{k=0}^{(j)}$ at $\omega\sim 0$ and at $\omega\gg\Omega_0$. A visible maximum occurs only at $\omega\approx 1.5\Omega_0$. This is confirmed also by plot for the function $\mathrm{Im}[\epsilon_c/\epsilon(\omega)]$, which is presented in the inset at the top of Fig. 6 where we used $\Gamma=0.1$ and the same parameters as for the 3D plot. A similar tendency holds also for fluxon structures shown in Figs. 3–5.

IV. CONCLUSIONS

In conclusion, we have considered the structure of a fluxon lattice in a layered superconductor under a constant magnetic field applied parallel to the layers. The obtained solution of the system of nonlinear equations describes the interlayer phase difference $\varphi_{n,n+1}$, which behaves in a peculiar way compared to the field strength and anisotropy. The ordered structure is formed by chains of fluxons, which become disarranged at certain conditions. The calculated $\varphi_{n,n+1}$ is then used to explore the spectrum of small vortex and plasma oscillations. The spectrum Ω_k differs from the spectrum of small oscillations in a single Josephson junction. This difference is due to a contribution of the interlayer interaction. We obtain that the spectrum has a fine band structure showing gaps.

ACKNOWLEDGMENT

S.E.S. would like to thank R. Kleiner and A. Ustinov for fruitful discussions.

*Permanent address: Institute of Magnetism NANU, 36(b) Vernadskii av., Kiev, Ukraine.

[1] R. Kleiner, F. Steinmeyer, G. Kunkel, and P. Müller, Phys. Rev. Lett. **68**, 2394 (1992); R. Kleiner and P. Müller, Phys. Rev. B **49**, 1327 (1994); P. Müller, in *Festkörperprobleme, Advances in Solid State Physlcs*, edited by R. Helbig (Vieweg, Braunschweig, 1994), Vol. 34.

[2] K. Tamasaku, Y. Nakamura, and S. Uchida, Phys. Rev. Lett. **69**, 1455 (1992).

[3] C. C. Homes, T. Timusk, R. Liang, D. A. Bonn, and W. N. Hardy, Phys. Rev. Lett. **71**, 1645 (1993); D. N. Basov, T. Timusk, B. Dabrowski, and J. D. Jorgensen, Phys. Rev. B **50**, 3511 (1994); B. Koch, M. Durrler, H. P. Geserich, Th. Wolf, G. Roth, and G. Zachmann, in *Electronic Properties of High T_c Superconductors and Related Compounds*, edited by H. Kuzmany, M. Mehring, and J. Fink (Springer-Verlag, Berlin, 1990).

[4] A. M. Gerrits, A. Wittlin, V. H. M. Duyn, A. A. Menovsky, J. J. M. Franse, and P. J. M. van Bentum, Physica C **235-240**, 1117 (1994); Jae H. Kim, H. S. Somal, M. T. Czyzyk, D. van der Marel, A. Wittlin, A. M. Gerrits, V. H. M. Duijn, N. T. Hien, and A. A. Menovsky, *ibid.* **247**, 297 (1995).

[5] M. Tachiki, T. Koyama, and S. Takahashi, Phys. Rev. B **50**, 7065 (1994); S. E. Shafranjuk, M. Tachiki, and T. Yamashita, *ibid.* **53**, 15 136 (1996); **55**, 582 (1997); Y. Zha, K. Levin, and D. Z. Liu, *ibid.* **51**, 6602 (1995); S. V. Pokrovsky and V. L. Pokrovsky, J. Supercond. **8**, 183 (1995); M. J. Graf, M. Palumbo, D. Rainer, and J. A. Sauls, Phys. Rev. B **52**, 10 588 (1995).

[6] L. N. Bulaevskii, M. P. Maley, and M. Tachiki, Phys. Rev. Lett. **74**, 801 (1995).

[7] L. N. Bulaevskii, V. L. Pokrovsky, and M. P. Maley, Phys. Rev. Lett. **76**, 1719 (1996); L. N. Bulaevskii, M. P. Maley, H. Safar, and D. Dominguez, Phys. Rev. B **53**, 6634 (1996).

[8] L. J. Campbell, M. M. Doria, and V. G. Kogan, Phys. Rev. B **38**, 2439 (1988); S. N. Artemenko and A. N. Kruglov, Physica C **173**, 126 (1991); L. N. Bulaevskii, M. Ledvij, and V. Kogan, Phys. Rev. B **46**, 366 (1992).

[9] L. N. Bulaevskii and J. R. Clem, Phys. Rev. B **44**, 10 234 (1991); L. N. Bulaevskii, J. R. Clem, and L. I. Glazman, *ibid.* **46**, 350 (1991); A. F. Volkov, Physica C **192**, 306 (1991).

[10] L. I. Glazman and A. E. Koshelev, Physica C **173**, 181 (1991); Phys. Rev. B **43**, 2835 (1991); L. L. Daemen, L. N. Bulaevskii, M. P. Maley, and J. Y. Coulter, *ibid.* **47**, 11 291 (1993); Phys. Rev. Lett. **70**, 1167 (1993).

[11] P. Lebwohl and M. J. Stephen, Phys. Rev. **163**, 376 (1967); A. L. Fetter and M. J. Stephen, *ibid.* **168**, 475 (1968); I. O. Kulik, Zh. Eksp. Teor. Fiz. **51**, 1952 (1967) [Sov. Phys. JETP **24**, 1307 (1967)].

[12] R. Kleiner, P. Müller, H. Kohlstedt, N. F. Pedersen, and S. Sakai, Phys. Rev. B **50**, 3942 (1994).

[13] S. Sakai, A. V. Ustinov, H. Kohlstedt, A. Petraglia, and N. F. Pedersen, Phys. Rev. B **50**, 12 905 (1994).

[14] S. Sakai, P. Bodin, and N. F. Pedersen, J. Appl. Phys. **73**, 2411 (1993).

[15] T. Koyama and M. Tachiki, Phys. Rev. B **54**, 16 183 (1996).
[16] G. J. Dolan, F. Holtzberg, C. Feild, and T. R. Dinger, Phys. Rev. Lett. **62**, 2184 (1989).
[17] B. I. Ivlev and L. J. Campbell, Phys. Rev. B **47**, 14 514 (1993).
[18] Ch. Kittel, *Introduction to Solid State Physics* (Wiley, New York, 1971).
[19] O. K. C. Tsui, N. P. Ong, and J. B. Peterson, Phys. Rev. Lett. **76**, 819 (1996).